J. Fluid Mech. (1995), *vol.* 289, *pp.* 1–27

Three-dimensional vortex dynamics in a rectangular sudden expansion

By J. R. HERTZBERG[1] AND C. M. HO[2]

[1] Department of Mechanical Engineering, University of Colorado, Boulder, CO 80309-0427, USA

[2] Mechanical, Aerospace and Nuclear Engineering Department, University of California, Los Angeles, CA 90024-1597, USA

(Received 1 April 1993 and in revised form 28 October 1994)

A detailed experimental study of flow in a rectangular sudden expansion using both active and passive forcing techniques has been made. The configuration consists of a 2:1-aspect-ratio rectangular channel which undergoes a sudden expansion such that the backward-facing step height (h) is uniform, and equal to the minor side of the inlet channel. Passive forcing was provided by the system geometry; the rectangular vortex rings formed in the shear layer of the expanding jet undergo self-induction, deforming the jet cross-section and introducing transverse velocities not found in plane or axisymmetric configurations. Active forcing was induced by periodic fluctuations in the system flow rate at the jet natural frequency. This served to enhance the unusual three-dimensional effects and phase-lock the flow for ensemble analysis. The results presented here include a description of the evolution of an isolated vortex in this configuration obtained from flow visualization of a suddenly started jet, as well as forced steady-state three-component velocity measurements which are used to characterize the flow field. The evolution of a rectangular vortex ring in the jet shear layer is traced, and both fluctuating and time-constant transverse velocities are related to the passage of the vortex structures.

1. Introduction

The control of mixing processes is of vital importance in combustion, other chemically reacting flows, and in heat transfer applications. Recent advances have been made in the control of mixing using techniques which affect the behaviour of the coherent structures formed in shear layers (Ho & Huerre 1984). These vortex structures are in turn responsible for the entrainment of fluid into the shear layer, and thus are responsible for controlling the mixing process. Both passive techniques, which act through the system geometry, and active techniques, which involve flow perturbations in time, have been demonstrated. These techniques have been examined in the context of two-dimensionally symmetric configurations, and in unconfined three-dimensional flows, but further understanding of these techniques in confined, three-dimensional geometries is required for useful application. A rectangular sudden expansion has been chosen for study for its relevance to ramjets and other dump-type combustors.

While this precise configuration has not been examined previously, it has features in common with several well-studied flows: asymmetric jets, backward-facing steps, and symmetric sudden expansions. Active perturbation in the form of acoustic excitation or vibrating flaps have been applied to these well-studied flows both for control of the vortex structures and for analysis using phase-locked techniques. A brief review of studies in these areas follows.

Passive control of mixing is generally applied in jets through the use of asymmetric nozzle geometries which azimuthally perturb the vortex structures in the jet shear layer, resulting in self-induced deformations and complex pairing interactions. These effects in turn result in higher entrainment and mixing. The term 'asymmetric' is used here to refer to jets which are neither axi- nor plane-symmetric. The transverse azimuthal perturbations range from nearly circular elliptic jets to high-aspect-ratio rectangular jets to jets of arbitrary cross-section: triangular, star-shaped, jets with tabs, etc. All of these jets display certain characteristics in common: deformation of the jet cross-section with downstream distance, and entrainment which is at least equal to that of circular jets, and in some cases several times larger than that of circular jets.

Studies of the deformation of elliptic water jets in air have been reported as early as 1879, by Lord Rayleigh, but studies of asymmetric single-phase jets date to Sforza, Steiger & Trentacoste (1966). These studies of primarily high-aspect-ratio (> 10) rectangular jets noted the phenomenon of axis switching, wherein the minor axis of the jet spreads more rapidly than the major axis. These rectangular jet studies also mentioned the possibility that their results were due to the deformation of rectangular vortex rings surrounding the jet. Other early asymmetric jet studies were motivated by the use of rectangular nozzles for vectoring, thrust augmentation and noise reduction on aircraft engine exhausts (Viets 1972, 1976; Crighton 1973; Hiley, Wallace & Booz 1976; Sfeir 1976, 1979; Hoyt & Taylor 1978). This work was continued with the investigation of high-aspect-ratio and supersonic rectangular jets (Krothapalli, Baganoff & Karamcheti 1980, 1981; Hsia *et al.* 1983; Krothapalli 1985). Jet deformations involving corners which become planar with downstream distance, or axis switching in the case of elliptic jets, have been documented in each of these asymmetric flows at both low and high Reynolds numbers.

In general, the deformation of asymmetric jets can be attributed to the self-inductive behaviour of coherent structures formed in the shear layers, although Pollard & Schwab (1988) and Quinn (1992) suggest that details of the inlet flow can have a dominant effect. Ho & Gutmark (1987) have observed the vortex structures in laminar elliptic jets to behave in a manner consistent with that of isolated vortex rings. Non-circular vortex rings deform according to self-induction, the effect of one portion of the vortex ring on another. This causes the regions of the vortex rings with higher curvature to convect ahead of the rest which in turn increases the curvature of the lagging portions. These portions then overtake and decrease the curvature of the initial high-curvature sections (Kambe & Takao 1971). As a result, the elliptical shape is restored, but the axis which was initially the minor axis has become the major axis, and the motion begins again. The deformation of vortex rings formed as structures in the shear layers of asymmetric jets can thus deform the jet cross-section, and entrain substantially more fluid into the jet (Ho & Gutmark 1987).

Active forcing of the vortex structures in elliptic jets can cause further deformation of the jet structure as the complex pairing interactions are manipulated. Hussain & Husain (1989) and Husain & Hussain (1991) have performed an extensive study of vortex dynamics in forced elliptic jets.

The confined, forced rectangular jet under consideration here is thus expected to spread more rapidly on the minor axis. However, the effects of confinement on the developing shear layers are expected to be severe, as they are in the well-studied cases of confined flow over backward-facing steps and in axisymmetric sudden expansions. Eaton & Johnston (1981) reviewed unforced flow over backward-facing steps, reporting reattachment lengths from 5 to 15 step heights, with many values in the range from 6 to 8. The recirculation zone length is found to be sensitive to upstream

boundary layer conditions, as well as the overall expansion ratio. Active forcing of reattaching shear layers using flaps (Roos & Kegelman 1986) and acoustic excitation (Bhattacharjee, Scheelke & Troutt 1986) has demonstrated that the recirculation zone length can be manipulated by appropriate encouragement or discouragement of pairing in the free shear layer before reattachment.

Axisymmetric expansions have also been extensively studied, and are reviewed briefly in Morrison, Tatterson & Long (1988). They differ from backward-facing steps in that the central jet flow has a finite potential core length, and thus the development of the shear layer is limited both by the outer walls and the centreline. Reported recirculation zone lengths tend to be longer than similar backward-facing step flows, averaging 8 to 9 step heights. A sudden expansion of a well-developed square duct flow was studied by Nakao (1986) who found that the streamwise vortices associated with square ducts were suppressed by the expansion.

Nominally two-dimensional flows have been found to have significant three-dimensional secondary flows, even for aspect ratios of more than five. Cherdron, Durst & Whitelaw (1976) found three-dimensional flows in a plane symmetric expansion at aspect ratios up to 8, the largest measured. In addition, unequal recirculation zone lengths were found.

A limited amount of research has been performed on deliberately asymmetric expansions. Stevenson, Thompson & Craig (1984) mention a study of flow over a rectangular backward-facing step of aspect ratio one, in which considerable three-dimensionality was found. Foss & Jones (1968) and Holdeman & Foss (1975) studied secondary flows in rectangular jets which are bounded on their short sides. Measurements of vorticity and velocity showed that the development of secondary flow was due to the distortion of vortex loops surrounding the jet. The interaction of vortex structures and the secondary flow was examined by Shimuzu, Ishii & Wada (1986) in a numerical simulation of a forced bounded rectangular jet.

Asymmetric expansions have begun to be applied in combustion systems. The Coanda effect found in an off-centre circular expansion has been studied by Wu *et al.* (1988), and used to generate transverse flows and high turbulence for the stabilization of coal flames. Grinstein & Kailasanath (1993) have performed numerical simulations of reactive square jets. Schadow & Gutmark (1992) give a brief review of their studies of reacting and non-reacting flows in a variety of asymmetric configurations. Triangular and square inlet ducts and jets have been studied, and it was found that the combination of large-scale structures from the flat sides of the jets and small scales from the corners reduced combustion instability and extended flame stabilization limits. However, transverse flows in these configurations have not been studied.

An extensive survey of the flow field in a suddenly expanded low-aspect-ratio rectangular jet has been made in order to determine the effect of passive and active forcing on the recirculation zone structure in isothermal flow. Time-averaged results are reported in Hertzberg & Ho (1992). Time-resolved results are presented here, including flow visualization of a starting jet vortex ring in this configuration, as well as ensemble-averaged laser Doppler velocimetry (LDV) measurements of three velocity components, phase-locked to a forced velocity perturbation in the exit flow.

2. Experimental description

The experiments were carried out in a vertical water channel consisting of a 2:1 aspect-ratio rectangular jet (7.62×3.81 cm) which underwent a sudden expansion with uniform step height (h) equal to the minor channel width (figure 1). Screens were placed

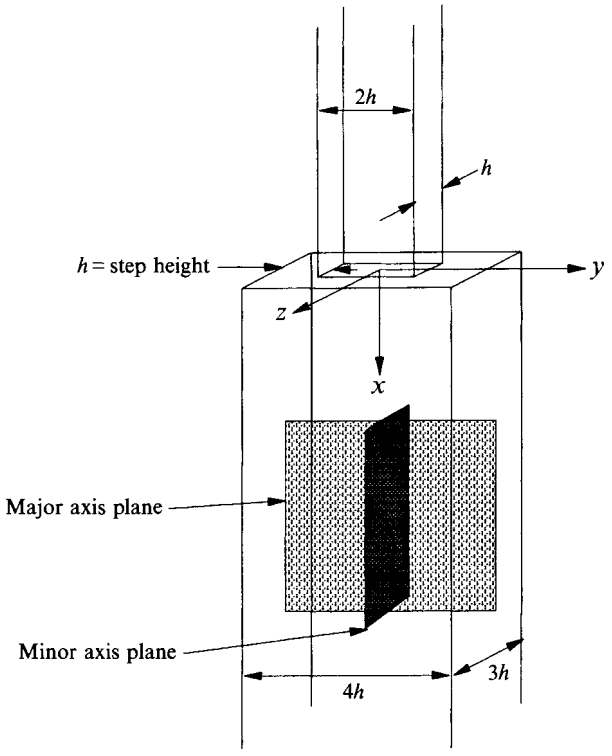

FIGURE 1. System configuration

in the channel upstream of the expansion at $x/h = -1, -2, -3$ to ensure uniform flow and a thin initial boundary layer. Coordinates are specified from the centreline of the jet in the plane of the expansion, with x as the streamwise direction, y along the major axis and z along the minor. The terms 'major' and 'minor' will refer to the orientation of the inlet channel flow, rather than the local jet orientation.

Two flows are presented here: a suddenly started 13 cm s^{-1} jet ($Re_h = 5000$) and perturbed (forced) steady-state flow at $Re_h = 8500$, where $Re_h = U_0 h/\nu$ and $U_0 = 21.6$ cm s^{-1} is the initial jet velocity measured at the centreline, $x/h = 0.5$.

The flow system for the suddenly started jet studies was equivalent to a blow-down type. The channel was filled with water and sealed at the top, at a height of 3.6 m. The channel exit was opened fully, below the water surface of the lower reservoir. The flow rate was controlled by bleeding air into the top of the channel, resulting in the 13 cm s^{-1} jet. Although quantitative measurements of the flow pattern were not made, video records show that the results were quite repeatable.

The steady-state flow was driven by a constant 3.6 m head system and the flow rate was controlled at the exit. The free-stream turbulence intensity was 1.1%. Active forcing was provided by a global pressure perturbation, created by passing a small portion of the exit flow through a computer-controlled rotating butterfly valve, resulting in an approximately sinusoidal 3% r.m.s. fluctuation in the initial jet velocity.

The hydrogen bubble technique was used to visualize the suddenly started jet. Stainless steel wire, 2 mm in diameter, was stretched across the entrance to the dump section, outlining the initial jet. Salt was added to the water to increase the bubble generation rate, and the circuit was completed by a copper plate placed in the pump reservoir. Forty volts d.c. was applied between the wires and the plate, and the results were recorded on video tape and Polaroid film. However, the flow is highly three-

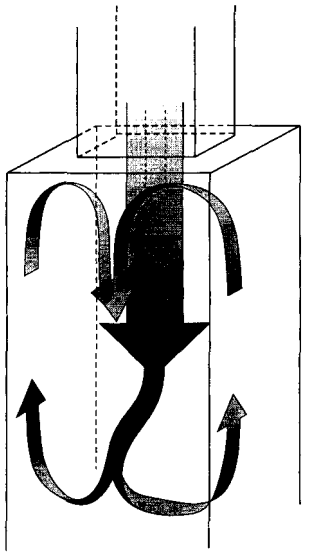

FIGURE 2. The flow configuration: a rectangular sudden expansion.

dimensional, and the two-dimensional recordings were found to be somewhat misleading. The interpretations in this paper are primarily from direct observation.

Quantitative velocity measurements of the flow under perturbed steady-state conditions were made with a two-component, frequency-shifted LDV system. The optics were the Dantek 55X three-beam system, with expansion and a 310 mm lens, resulting in a measurement volume of 1.1 by 0.09 mm. Two TSI IFA-550 counters were used. The analog output of the counters was then sampled at 100 Hz, with a 1 μs delay between channels. Measurements of near zero velocities were carried out in stagnant flow as an independent check on the system calibration. The individual data rates ranged from 5 kHz in the low-velocity regions to more than 20 kHz in the high-velocity regions. Examination of the raw data revealed that an assumption of continuous data was reasonable under these conditions, even in regions of high turbulence. Velocity bias effects are thus considered negligible (Durst, Melling & Whitelaw 1981; Stevenson, Thompson & Roesler 1986; Adams *et al.* 1984). Seeding was provided by the naturally occurring particulates in tap water, filtered to 5 μm. All data acquisition and the optics traversing mechanism were controlled by an IBM AT compatible. 32000 samples were collected at each location, and ensemble-averaged means were calculated, as well as the vorticity fields derived from the phase-locked velocity fields.

Measurements were taken in the major and minor axis half-planes, from 0.5 to 5.0 step heights downstream, on a grid with $0.1667h$ spacing. Measurement traverses were spaced twice as closely in y and z across the high-shear regions. Measurements in the boundary layers were not made. Data were also taken in transverse planes at $x/h = 0.5$ and $x/h = 3$, with the above spacing. U and V were measured simultaneously, in the $(+y, -z)$ quadrant, and U and W measurements were made in the $(+y, +z)$ quadrant. When the ensemble-averaged results were assembled, U was averaged from the two measurements. Discrepancies between the two measurements were less than 6% of U_0, indicating the symmetry of the flow.

The output from a Hall effect sensor on the rotating butterfly valve shaft was sampled within 1 μs of the analog velocity signals. This provided a timing reference to the forcing velocity perturbation. Since the perturbation frequency was 2 Hz and the sampling rate was 100 Hz, the forcing cycle was divided into 50 time bins which were

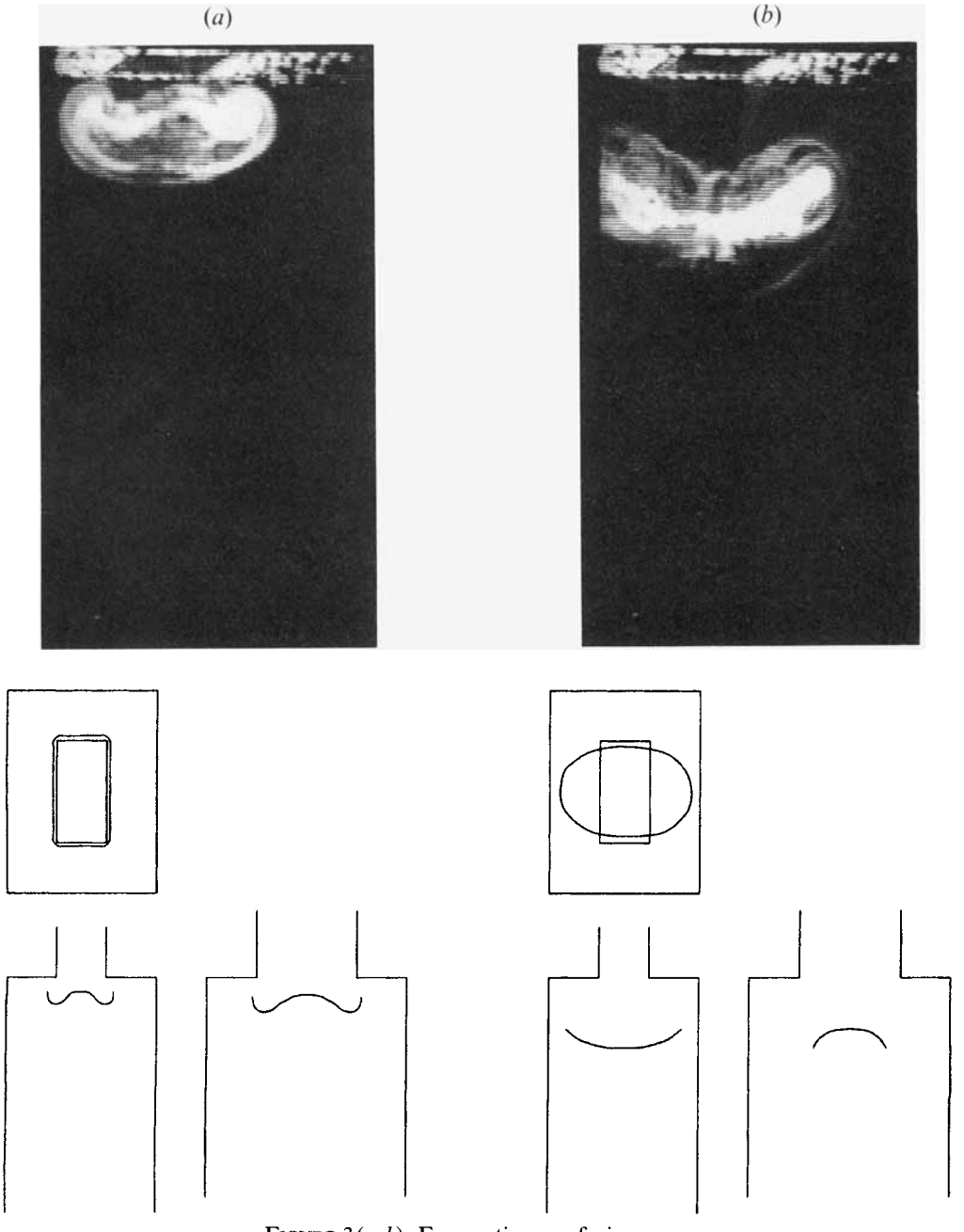

FIGURE 3(*a*, *b*). For caption see facing page.

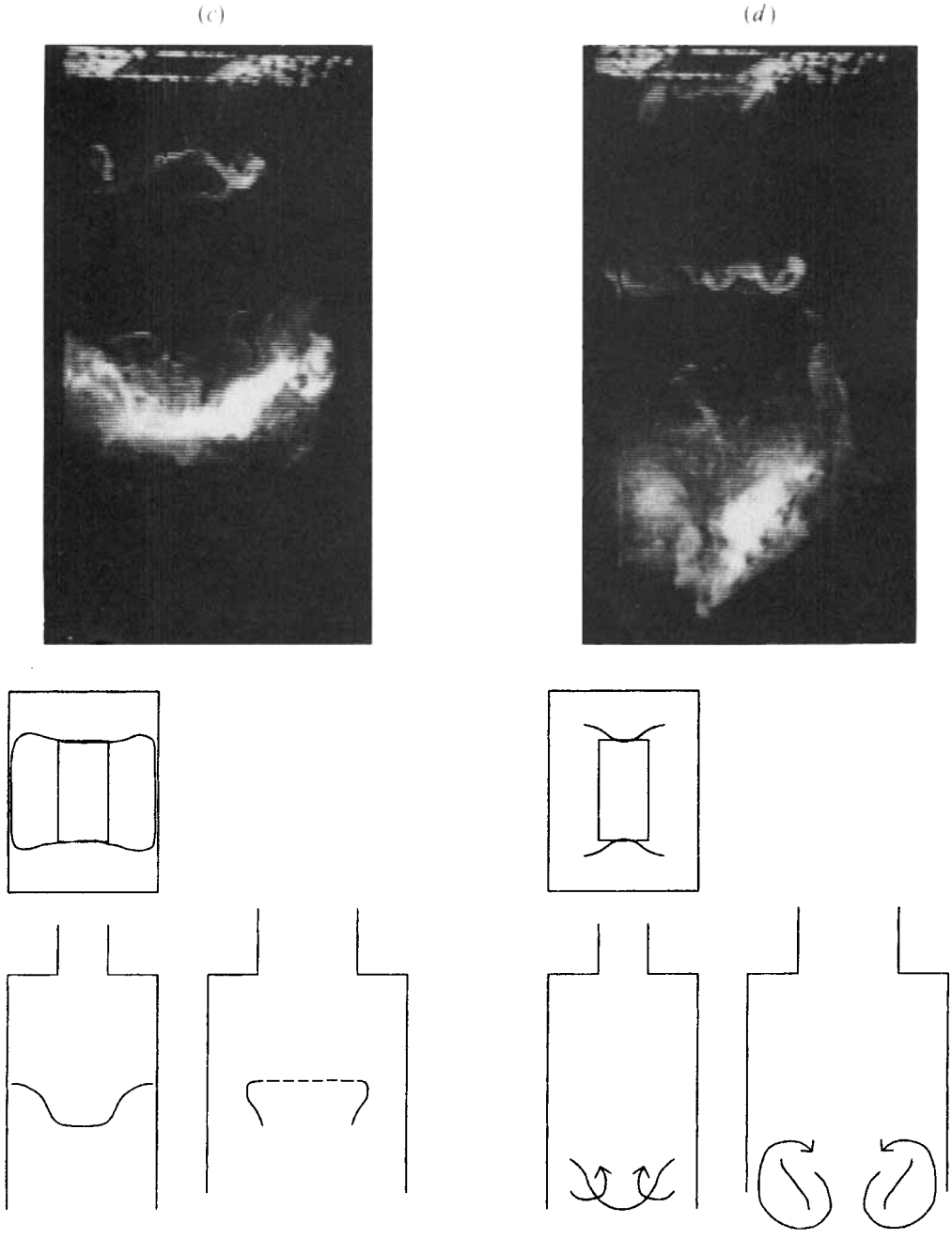

FIGURE 3. A suddenly started jet at (*a*) 0.60 s, (*b*) 1.67 s, (*c*) 3.17 s, (*d*) 4.33 s.

sequentially filled. At each location 654 cycles were ensemble averaged. All flow quantities presented in this paper are the ensemble-averaged results, with the exception of U_0, unless otherwise noted.

3. Results

3.1. *Time-averaged results*

A brief synopsis of the time-averaged data reported in Hertzberg & Ho (1992) follows.

A unique secondary flow was revealed in the regions behind the step of the rectangular sudden expansion, as shown in the schematic in figure 2. The jet spreads rapidly outward along the minor axis. The confining walls redirect this outward flow to be parallel to the major axis, into the outer corners of the recirculation zone. This fluid then recirculates back to the region behind the step, where it is carried perpendicular to the jet axis, into the region near the minor axis. Symmetry and confinement then act to redirect the secondary flow to be parallel to the jet flow. This results in positive axial flow everywhere in the minor axis plane, i.e. no recirculation zone. The reattachment length for the shear layer on the minor axis is much more difficult to define in the absence of recirculation, and could be interpreted to be zero. The suppression of recirculation in the minor axis plane demonstrates the importance of three-dimensional considerations. Results from two-dimensional flows suggest that the recirculation zone on the minor axis should be longer that on the major axis, owing to the higher expansion ratio. Instead, the fully three-dimensional geometry has eliminated the recirculation zone entirely.

3.2. *Isolated vortex ring deformation*

Since the global flow pattern in this configuration is believed to be related to the vortex dynamics of the coherent structures in the shear layers, the behaviour of an isolated vortex ring in this geometry was studied for clues to the behaviour of the forced, steady-state flow. Direct visualization of the coherent structures in the steady-state flow is difficult owing to the transitional nature of the shear layers. While the initial shear layers are laminar, they quickly become turbulent owing to interactions with neighbouring vortexes, dispersing any flow markers such as hydrogen bubbles or dye. In contrast, a vortex ring generated by suddenly starting the jet flow is easy to trace by marking a plug of fluid in the inlet channel with hydrogen bubbles. However, care must be taken in relating the behaviour of the isolated ring to the steady-state jet for several reasons. For instance, vortex ring behaviour is sensitive to the strength of the vortex, a quantity which is difficult to measure (and thus to match) in either an isolated ring or in a structure embedded in a shear layer. Also, in this geometry the confining walls dictate a secondary recirculating flow which must in turn affect the structures in the shear layer. Finally, the most important difference between an isolated vortex and coherent structures in shear layers is the lack of interaction with other vortices in the isolated case. Nevertheless, the effect of confinement on the isolated vortex ring should be similar to the behaviour of structures near the wall. This similarity is strengthened in our experiment by forcing the flow in the steady-state jet such that no vortex pairing is expected in the region between the sudden expansion and the end of the potential core.

The evolution of the vortex ring in the suddenly started jet is shown in figure 3. The view in the photographs is at a slight angle to the major axis of the jet, similar to the central view in the schematics. The ring is initially flat, but soon deforms as the corner regions convect ahead due to their high curvature (figure 3*a*). By 1.67 s, seen in figure

3(*b*), perturbations due to the corners have propagated around the ring, and the overall deformation of the ring becomes similar to an elliptic ring. The ring has switched axes, with the major axis now in the plane of the photograph. In an unconfined vortex ring at this stage the sections at the ends of the new major axis with their now higher curvature would overtake the rest of the ring. However, in the confined flow here the walls prevent this. The next figure, 1.5 s later (figure 3*c*), shows the centre position of the major sides continuing to lead while the minor sides are stretched and intensified along the wall. This results in the hydrogen bubbles being convected away, and the ring portions along the wall become invisible. A second vortex ring in the jet shear layer has now appeared. The final figure in the sequence shows that the primary vortex ring has evolved into two diffuse V-shaped lines with indeterminate end points. Owing to the inward inclination of the apex of the V, the fluid rotation appears in the front view to be counter to the original vortex. Soon after this stage the flow becomes completely turbulent.

These observations demonstrate that the confining walls have a large effect on the isolated vortex ring. This in turn suggests that the precise geometry is important. With a slightly larger step size the walls might not have seriously interfered with the evolution of the ring.

3.3. *Steady-state jet results*

While the dynamics of an isolated vortex ring in this configuration cannot be expected to mimic the behaviour of vortex rings formed in the shear layer surrounding a steady-state jet, certain parallels can be drawn. For instance, the results from the suddenly started jet suggests that in the steady-state case the recirculation zone on the minor axis will be shorter than the major, as self-induction of the vortex rings causes the jet to spread more rapidly on the minor axis. Also, the ring deformation should result in streamwise vorticity. These features do appear in the forced steady-state results, as well as other effects due to the asymmetry and confinement.

The choice of a forcing frequency was based on an analysis of the unforced case as a free jet. The shear layer instability mode and the jet column mode are both of interest; however, owing to optical access constraints, which are much more severe in this three-dimensional configuration than in two-dimensional expansions, the initial momentum thickness of the shear layer at the expansion plane could not be measured. Measurements commenced at $x/h = 0.5$, and the dominant frequency in the shear layer for the unforced case at this location was 8 hz. Based on the measured convection speed U_c of the vortex structures in the forced case (discussed subsequently), $x/h = 0.5$ is approximately one wavelength of the dominant perturbation downstream of the expansion. Since four wavelengths are required for the first vortex merging to occur under these conditions (Ho & Nosseir 1981), the observed fluctuation at 8 Hz must necessarily be the initial shear layer instability.

The dominant frequency found at the end of the potential core in the unforced case was 2 Hz. This implies that two vortex mergings take place between the expansion plane and the end of the potential core. This jet column mode leads to a Strouhal number of $fD_e/U_0 = 0.56$ where D_e is the diameter of a circular jet of equal area. The forcing perturbation was thus chosen to match both the jet column mode and the second subharmonic of the initial shear layer mode. In addition, by forcing at the natural frequency of the coherent vortices in the downstream region the structures can be tracked farther. This forcing frequency was also found to increase the unusual positive flow near the minor axis walls (Hertzberg & Ho 1992) during a preliminary study of other forcing frequencies. Owing to the complexity of the flow field, only one forcing condition was studied in detail.

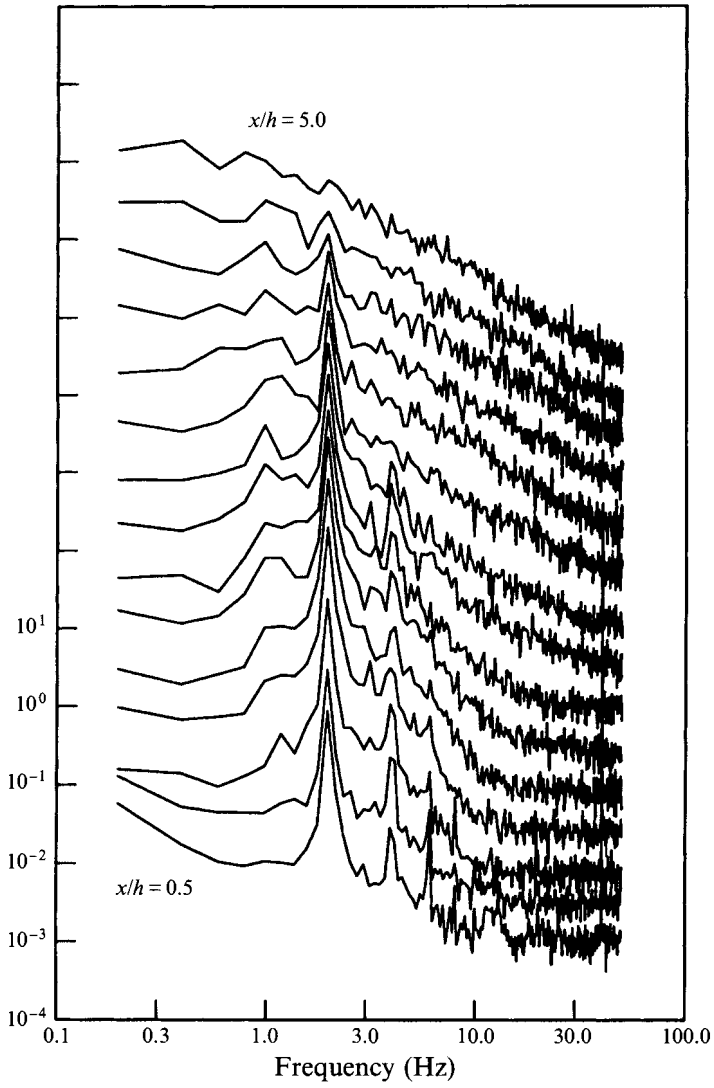

FIGURE 4. Development of the streamwise velocity spectra, at $x/h = 0.5$, bottom trace, and from $x/h = 0.67$ to 5, top trace, in increments of $0.33h$.

The development of the U velocity spectrum on the centreline is shown in figure 4. At $x/h = 0.5$ the perturbation at 2 Hz dominates, with small harmonic peaks at 4 and 6 Hz seen. At the end of the potential core, $x/h = 3$, the peak at the forcing frequency has grown, and a subharmonic at 1 Hz has appeared, suggesting the possibility of a pairing process. However, a pairing interaction is not expected since in free shear layers the first pairing does not occur until approximately four wavelengths downstream. The location of the 1 Hz subharmonic corresponds to only two wavelengths of the forced perturbation. By the end of the measurement region, the prominent peaks have vanished, and the spectrum is that of well-developed turbulence.

However, the development of the shear layers cannot be inferred from the centreline behaviour, and in fact the evolution of fluctuations in the major axis plane differs significantly from that on the minor axis. Figure 5 shows the evolution with downstream distance of the integral across the shear layer of energy of streamwise

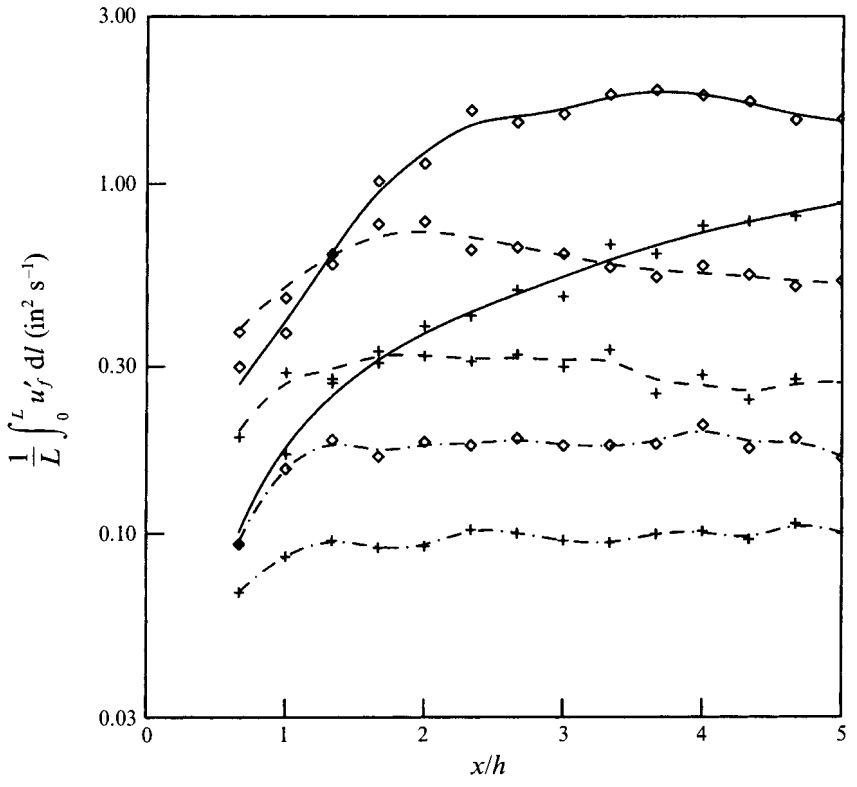

FIGURE 5. Spectral power density at specific frequencies, integrated across the shear layers: $(1/L)\int_0^L u_f' dl$). ◇, major axis plane; +, minor axis plane; ———, energy at forcing frequency; –·–·–, energy at 2× forcing frequency; ——, energy at 1/2 forcing frequency.

velocity fluctuations at specific frequencies: $(1/L)\int_0^L u_f' dl$, where u_f' is the r.m.s.[2] amplitude of fluctuations at frequency f, and $l = y$ and $L = 1.83h$ for the major axis data, while $l = z$ and $L = 1.33h$ for the minor axis. These data are thus normalized by the transverse extent of the velocity measurements, but not by the initial momentum thickness, which is assumed to be uniform azimuthally. As expected from forced free shear layer results, energy at the forcing frequency reaches a maximum early on, and then decays slowly, although the amplitudes in the minor axis plane are lower than in the major axis plane. The behaviour of the subharmonic of the forcing frequency is more interesting, in that the major axis value reaches a peak at $x/h = 3.5$, while the minor axis value increases throughout the measurement region. The saturation of the subharmonic eigenfunction (Ho & Huang 1982), coupled with the prominence of a small subharmonic peak in the centreline spectra again suggests the possibility of a pairing interaction on the major axis between $x/h = 3$ and 5, and none on the minor axis. However, since the forcing frequency corresponds to the dominant frequency at this location in the unforced flow, a pairing interaction is not expected, and the evidence is not conclusive. Instead, it is possible that the recirculation zone on the major axis is simply contributing to low-frequency unsteadiness and overall higher fluctuations.

The specific frequency energy contents on the minor axis are lower than those on the major axis, and this is also reflected in the fact that the time-averaged streamwise fluctuations are lower on the minor axis than on the major. It is interesting to note that

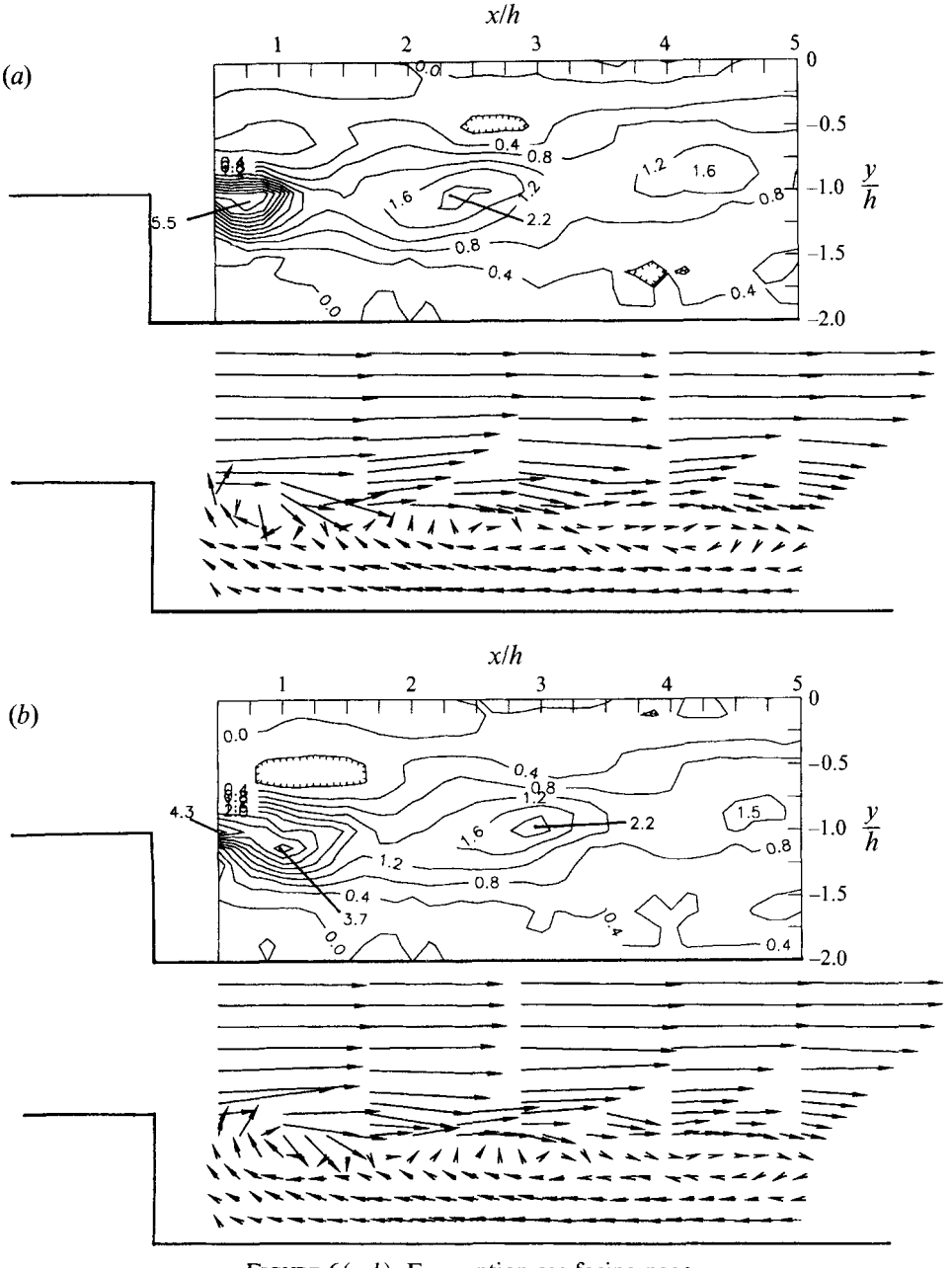

FIGURE 6(*a*, *b*). For caption see facing page.

significantly higher fluctuations on the major axis are *not* typically found in free elliptic or rectangular 2:1 aspect ratio jets. Ho & Gutmark (1987) studied an elliptic jet at $Re = 7.8 \times 10^4$, Husain & Hussain (1991) studied excited and unexcited elliptic jets at $Re = 3.2 \times 10^4$ and Tsuchiya, Horikoshi & Sato (1986) studied a rectangular jet at $Re = 1.5 \times 10^4$. In all three studies, peak fluctuation levels were similar on the major and minor axes, although the distribution varied with forcing. This demonstrates the effect of confinement on the turbulence properties of the flow. Troutt, Scheelke & Norman (1984) found that the reattachment of a turbulent shear layer in backward facing step

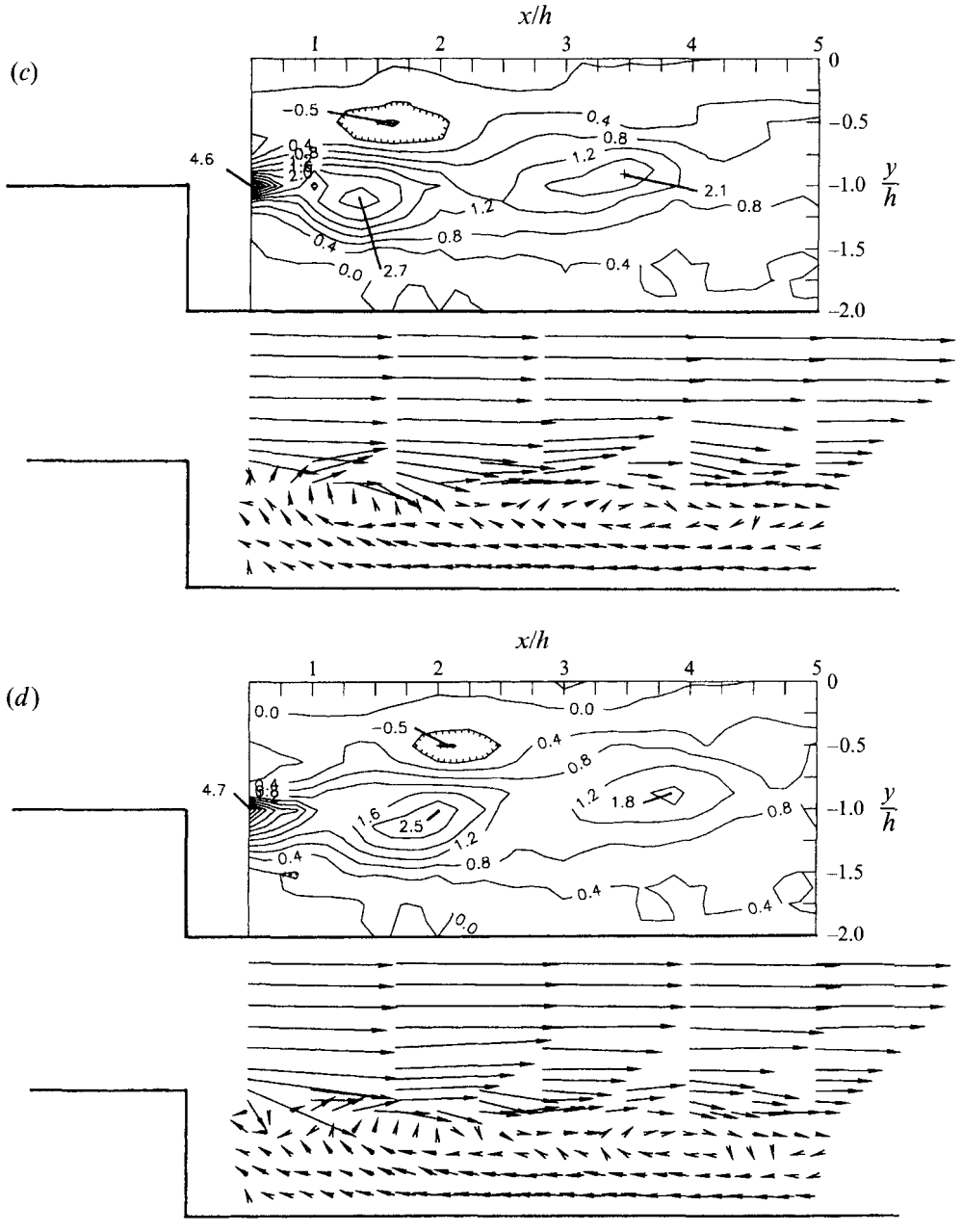

FIGURE 6. Velocity vectors U and V and contours of $\omega_z h/U_0$, in the major axis plane, at forcing phase (*a*) 0°, (*b*) 90°, (*c*) 180°, (*d*) 270°. Contour interval = 0.4.

flow appeared to inhibit the pairing process, rapidly reducing the turbulence intensity. Thus the flow on the minor axis is behaving in an 'attached' fashion, while the flow on the major axis may still be considered to be a free shear layer at this location.

3.3.1. *In the symmetry planes*

Figures 6 and 7 show selected velocity vectors and vorticity contours at four phases during the forcing cycle in the major and minor axis planes. All vector plots are scaled

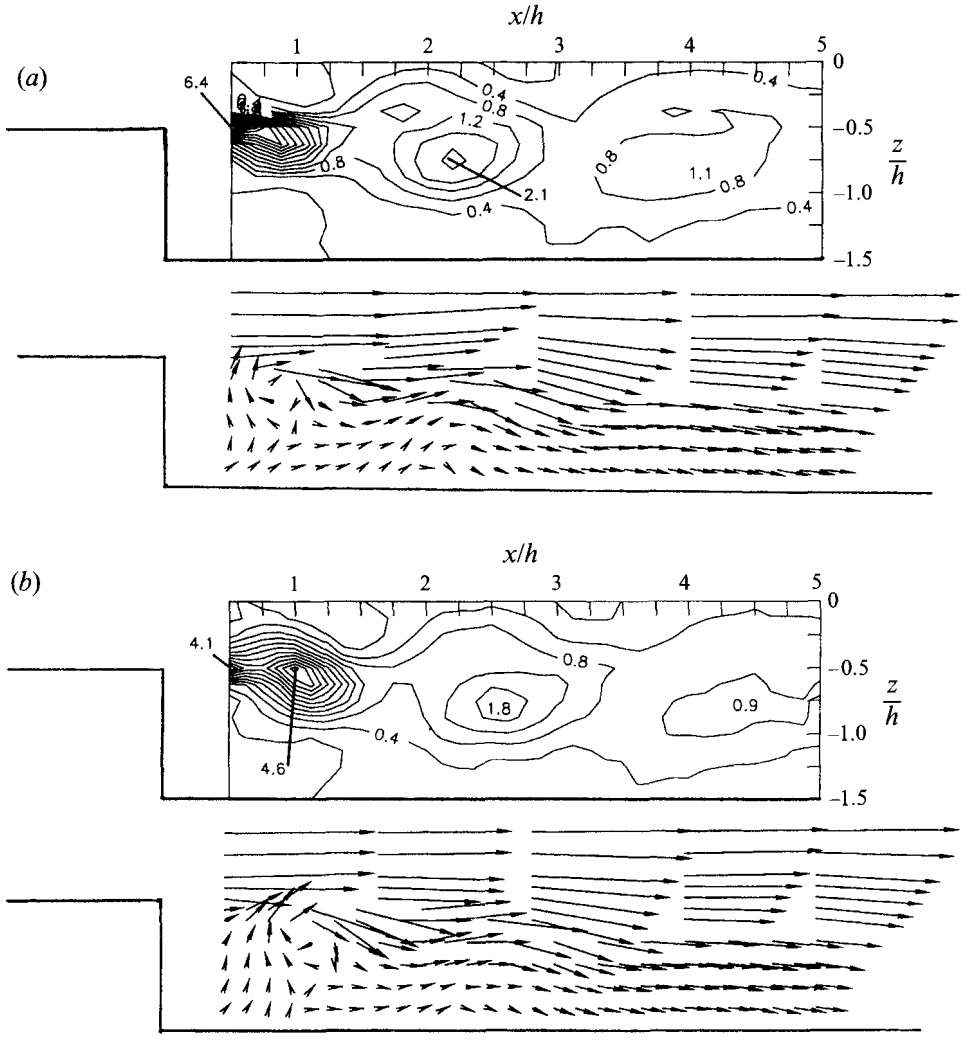

FIGURE 7(*a*, *b*). For caption see facing page.

by 0.2; a vector with a magnitude of $1h$ s^{-1} (where h is the step height) is represented by an arrow $0.2h$ in length. The vorticity field is calculated from the velocity field. Zero degrees has been defined to be at the peak velocity of the approximately sinusoidal perturbation, measured at $x/h = 0.5$. Circulation was not calculated; since vorticity is distributed throughout the shear layer, the circulation of a vortex structure would be quite sensitive to the exact contour chosen for integration.

The unique secondary flow is seen in the presence of a recirculation zone on the major axis, and the absence of recirculation on the minor axis. In figures 6 and 7, the velocity field of one half of the symmetry plane is shown, as well as normalized vorticity isocontours. The jet flow is seen in the top half of the figure, with the recirculation zone below, downstream of the step. As the amplitude of the perturbation at the forcing frequency grows with downstream distance, the effect can be seen in the magnitude of the velocity vectors in the jet, while in the recirculation zone on the major axis (figure 6), the amplitude of the phase-locked flow fluctuations near the wall remains on the order of 1% of U_0 throughout the measurement region.

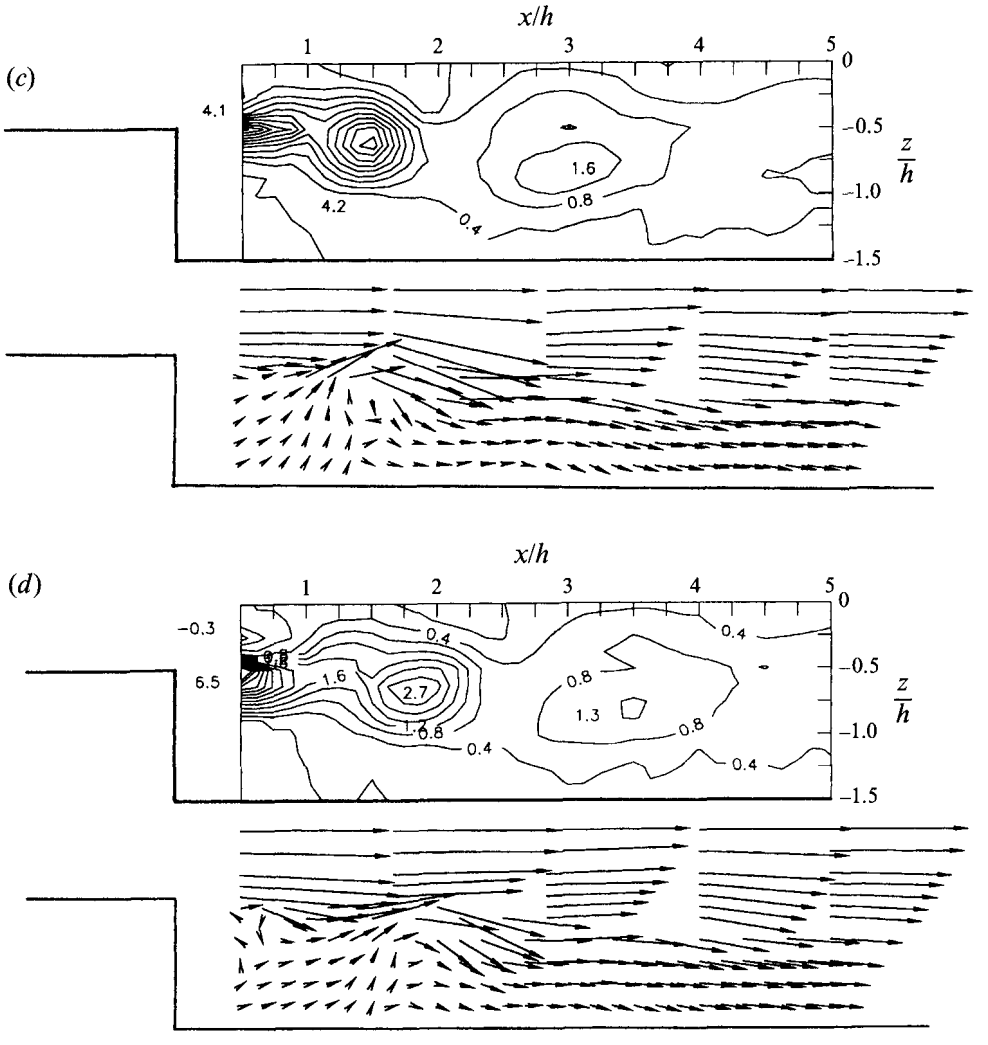

FIGURE 7. Velocity vectors U and W and contours of $-\omega_y * h/U_0$, in the minor axis plane, at forcing phase (*a*) 0°, (*b*) 90°, (*c*) 180°, (*d*) 270°. Contour interval = 0.4.

The lack of recirculation behind the backward facing step on the minor axis is the most unusual feature of this flow. Figure 7 shows that the only negative streamwise velocities on the minor axis are found just downstream of the step, and are associated with the passage of a vortex structure. Immediately downstream of the step, the velocities are low, but by $x/h = 3$ there is significant positive streamwise velocity close to the wall throughout the forcing cycle, indicating the rapid spread of the jet on the minor axis, and the rapid reattachment of the shear layer.

Note that on the major axis most of the transverse velocities (flow in the y-direction) are associated with the passage of the vortex structures. They are confined to the centre of the shear layer, with the exception of the region behind the step, from $x/h = 0$ to 1.5. There the bulk recirculating flow is deflected by the back of the step towards the jet. This flow pattern is consistent with flows behind two-dimensional backward facing steps, and in two-dimensional sudden expansions. Integration of v over the major axis plane at each phase reveals that the outward (away from the centreline) flow is

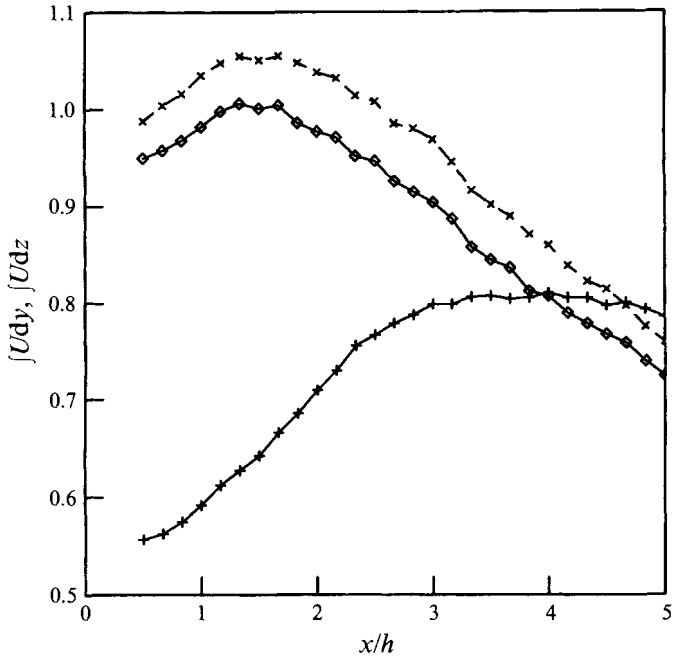

FIGURE 8. Time-averaged mass flow rates in the major and minor axis planes: ◇, major axis total $\int_0^{2.0} \bar{U}/U_0\,\mathrm{d}y/h$; ×, positive mass flow rate, major axis, $\int_0^{2.0} \bar{U}/U_0\,\mathrm{d}y/h > 0$; +, total minor axis $\int_0^{1.5} \bar{U}\,\mathrm{d}z/h$.

balanced by inward flow for most of the forcing cycle, although the inward flow is greater than the outer by 35% at 90° through the cycle.

In contrast, the transverse (w) flow in the minor axis plane (figure 7) appears dominated by the passage of the vortex structures in the entire region behind the step, up to $x/h = 3$. Note the strong inward flow behind the step, which appears to be due to entrainment into the vortex structure. Downstream of $x/h = 3$ a marked outward flow is evident across the entire channel, although influence of the vortex structures can still be seen. Integration of w over the minor axis plane shows that overall the outward flow is two to four times the inward flow. This feature is in agreement with results from free elliptic jets (Ho & Gutmark 1987) which showed that faster spreading and higher entrainment on the minor axis was due to the azimuthal deformation of the vortex structure in the shear layer.

In this confined case, the increased entrainment on the minor axis is demonstrated by figure 8. This figure is derived from time-averaged data, and shows that the flow rate in the minor axis region grows rapidly until $x/h = 3$ and then stabilizes, while the flow rate in the major axis region reaches a peak at $x/h = 1.5$ and then declines to a value below that of the minor axis plane. Note that these values are not normalized by the width of the area integrated. Thus the factor of two difference between the major and minor axes at $x/h = 0.5$ is consistent with the fact that the jet is initially twice as wide in the major axis plane. The amount of fluid recirculated is represented by the difference between the total and the positive flow rate in the major axis plane. This quantity remains constant with x/h. That the flow rate in the major axis region declines to a value below that of the minor axis region, while the overall flow rate remains constant (Hertzberg & Ho 1992) indicates that significant streamwise momentum which was originally carried in the major axis region is transferred to the minor axis

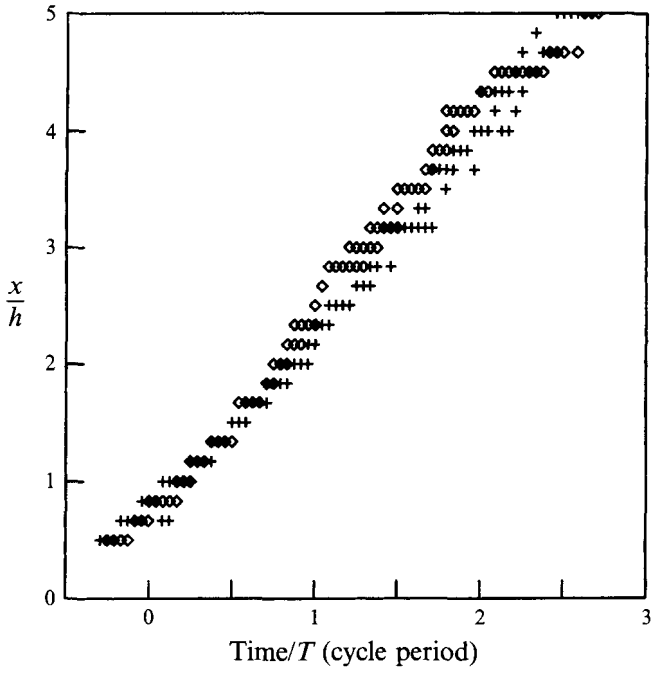

FIGURE 9. Position of peak vorticity: ◇, major axis plane; +, minor axis plane.

region. The most likely mechanism for transport of this momentum from the major to the minor axis region is the secondary flow system, with its significant transverse velocities. This point is illustrated later by the transverse plane velocity data.

The formation and evolution of the vortex structures in the shear layer on both the major and minor axes are clearly seen in figures 6 and 7. One vortex is generated during each forcing cycle, which is consistent with the moderate forcing intensity of 3%. The vortex does not appear to be the result of upstream pairing, in agreement with the spectra (figure 5) which showed that both the forcing frequency and its first harmonic saturate in the measurement region. Although observation of the behaviour of the structures in the downstream region is subject to the smearing effect of phase jitter, the footprint of an 'average' structure remains clear enough to be tracked to the end of the measurement region, even though the structures are no longer evident in the centreline spectra by $x/h = 5$ (figure 4).

The trajectory of the vortex cores in the major axis plane remains essentially on a line with the edge of the step, as was seen in the isolated vortex flow visualization. In contrast, the vortex cores, in the minor axis plane (figure 7) move outward towards the walls, although the dramatic wall interaction seen in the suddenly started jet case (figure 3) is not observed here. This may be due to the secondary flow which is developed in the steady-state jet acting as a buffer between the spreading jet flow and the wall.

Note that caution must be taken when examining the vortex structures as represented by apparent rotation of the velocity vectors. Although the vectors seem to rotate about points of zero velocity, the vortex centres are actually being convected in the shear layer with non-zero velocity. The speed of the vortex cores in the major and minor axis planes have been determined by plotting the position of the peak vorticity through 2.5 forcing cycles, the time it takes one structure to convect the length of the measured region. As can be seen in figure 9 the speeds of the vortex cores in both the

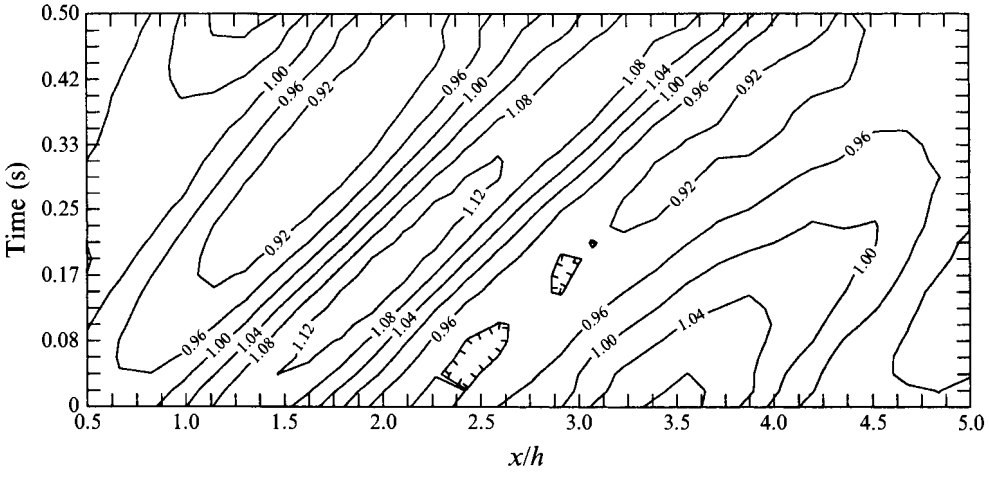

FIGURE 10. Streamwise velocity on jet centreline.

major and minor axes are fairly uniform. The stepwise appearance of the data is due to the limited resolution in x. A linear least-squares fit gives speeds of $U/U_0 = 0.66$ for both major and minor axes. The speed of the perturbation on the centreline correlates well with the vortex core speeds. Figure 10 is a contour plot of U in time and along the jet centreline. The propagation speed of the peak velocity can be graphically determined from the slope of the linear contours to be $U/U_0 = 0.72$. By comparison, Troutt *et al.* (1984) report a convection speed of $0.58U_0$ for vortex structures in their turbulent backward facing step flow.

While the azimuthal deformation of the vortex ring in the x-direction was clearly visible in the isolated vortex case, comparison of the locations of the vortex cores on the major and minor axes (figure 9) in the forced steady-state case reveals only slight variations. Before $x/h = 2.0$ the cores are travelling in phase. Then the vortex core on the major axis begins to lead slightly. This is consistent with the self-induction concept, since the ring has higher curvature near the major axis. However, one would expect higher deformation just after the vortex has been shed, as was observed in the isolated vortex ring case.

Figure 11 shows the evolution of the peak vorticity value with time. Although the circulation of the vortex structures would be interesting to examine, the distribution of vorticity would make the circulation quite sensitive to the precise contour chosen for integration. An additional scale in figure 11 shows the distance travelled, based on the measured average convection speed. The vortex cores on the major and minor axes begin with approximately the same strength, but the core on the major axis exhibits a two-slope behaviour, diffusing more rapidly until $x/h = 1.5$. Diffusion on the minor axis is more gradual, but exceeds that of the major axis after $x/h = 2$. This result is somewhat counter-intuitive, since the major axis core remains well away from any potential interaction with the walls, and the core remains within the region of higher spatial resolution, in the shear layer. The core on the minor axis might be expected to diffuse more rapidly as it moves away from the centreline; however, the data show that the major axis has faster diffusion in this region. A possible clue is provided by the entrainment data from figure 8 which show that the flow rate in the major axis plane increases until $x/h = 1.5$, and declines thereafter. The decline in flow rate on the major axis is not due to increased recirculation, but instead must be due to the outward

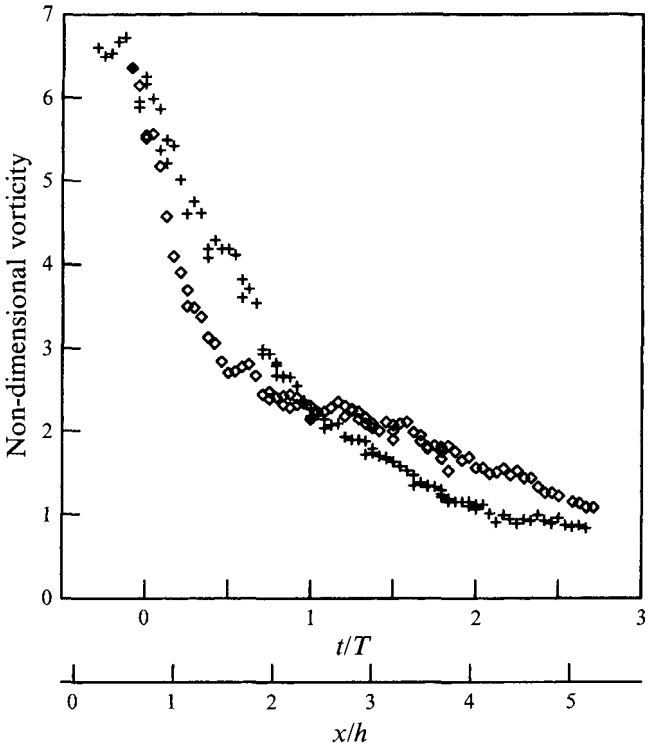

FIGURE 11. Peak vorticity in time: ◇, major axis plane; +, minor axis plane.

spreading jet in the minor axis region, and the resulting high entrainment demand in the upstream region of the minor axis. Thus on the major axis the entrained flow increases as the vorticity diffuses rapidly; when the flow rate declines, the vorticity diffuses more gradually. On the minor axis, entrainment increases monotonically, and the peak vorticity decreases smoothly. This suggests a coupling between the rate of diffusion of vorticity, and the flow rate entrained.

3.3.2. *In the transverse planes*

Vortex ring deformation can also be observed in the vorticity contours derived from the transverse plane data. Figure 12 shows the transverse velocity vectors, axial (U) velocity contours and normalized ω_x at $x/h = 0.5$. As the strong vortex core passes through the measurement plane between 270° and 0° through the cycle, positive ω_x can be seen in the shear layer at $y/h = 1.0$, $x/h = 0.4$, and a negative peak is found at $y/h = 0.8$, $z/h = 0.5$. This suggests that the shape corner of the vortex ring has begun to lead, resulting in the appearance of ω_x. This deformation corresponds to what is seen in the isolated vortex ring case early in its development, seen in figure 3(*a*).

Strong transverse flows in both V and W are associated with the passage of the vortex structure. At 0°, just after the structure has passed through the upper plane, there is inward flow across the shear layer, owing to the entrainment effect of the vortex. This inward flow diminishes through the cycle until it reverses, between 180 and 270°. Then the flow becomes outward across the shear layer, as the next vortex approaches.

In the downstream transverse measurement plane, at $x/h = 3$, shown in figure 13, the deformation of the average vortex ring is demonstrated in both the velocity field

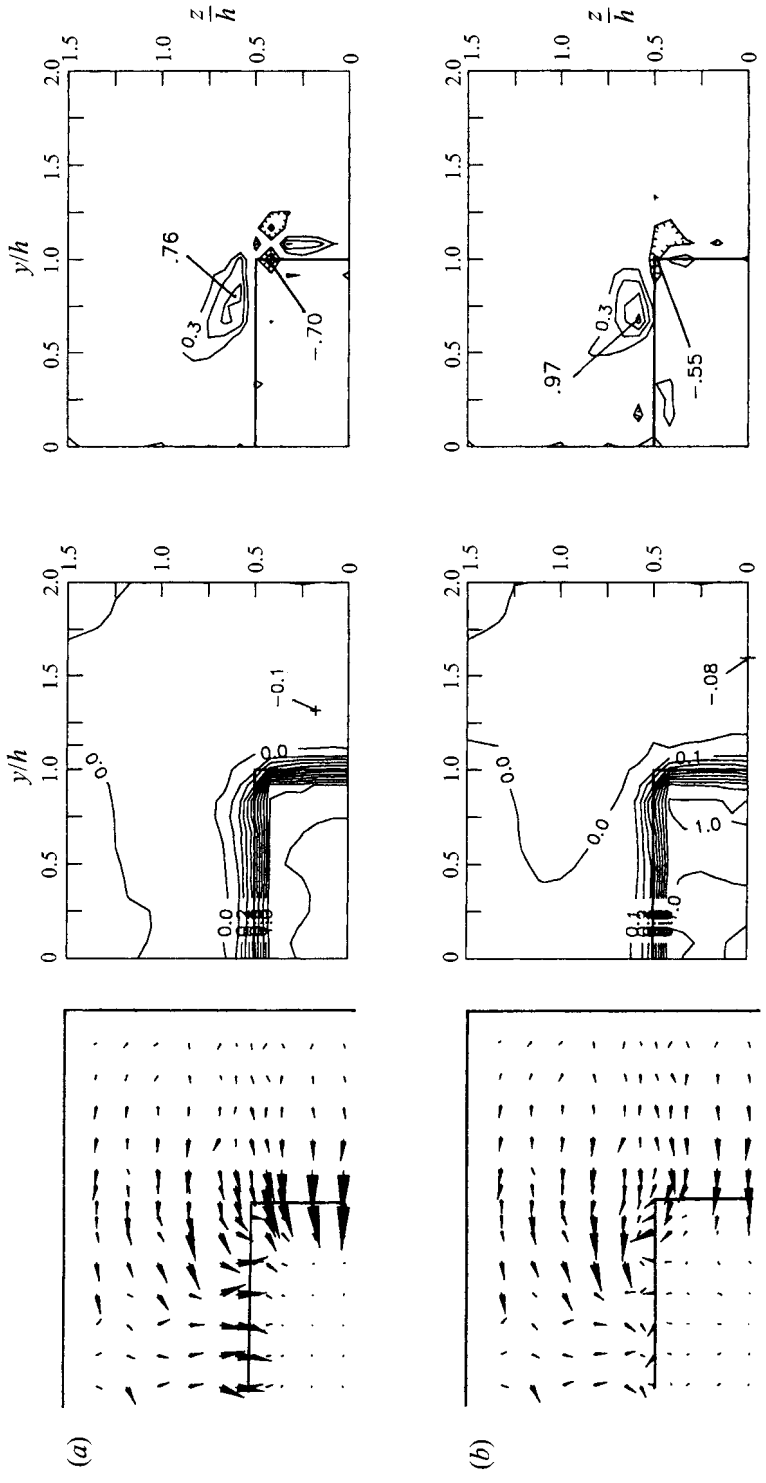
z/h
y/h
.76
0.3
-.70
.97
0.3
-.55
-0.1
0.0
-.08
0.1
1.0
(a)
(b)

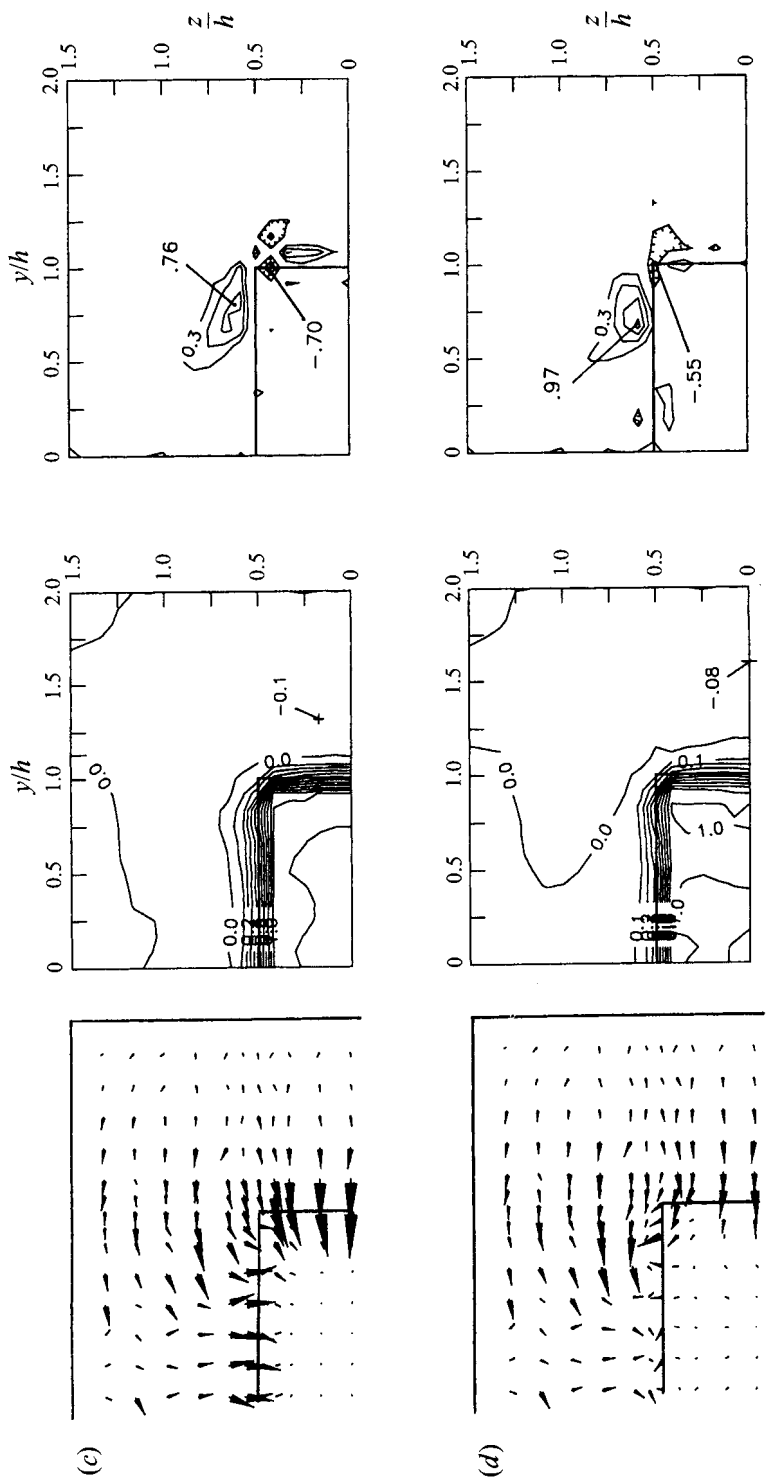

FIGURE 12. Velocity vectors V and W (left plots), contours of U/U_0 (middle plots) (contour interval = 0.1), and contours of $\omega_x h/U_0$ (right plots) (contour interval = 0.2), at $x/h = 0.5$: (*a*) 0°, (*b*) 90°, (*c*) 180°, (*d*) 270°.

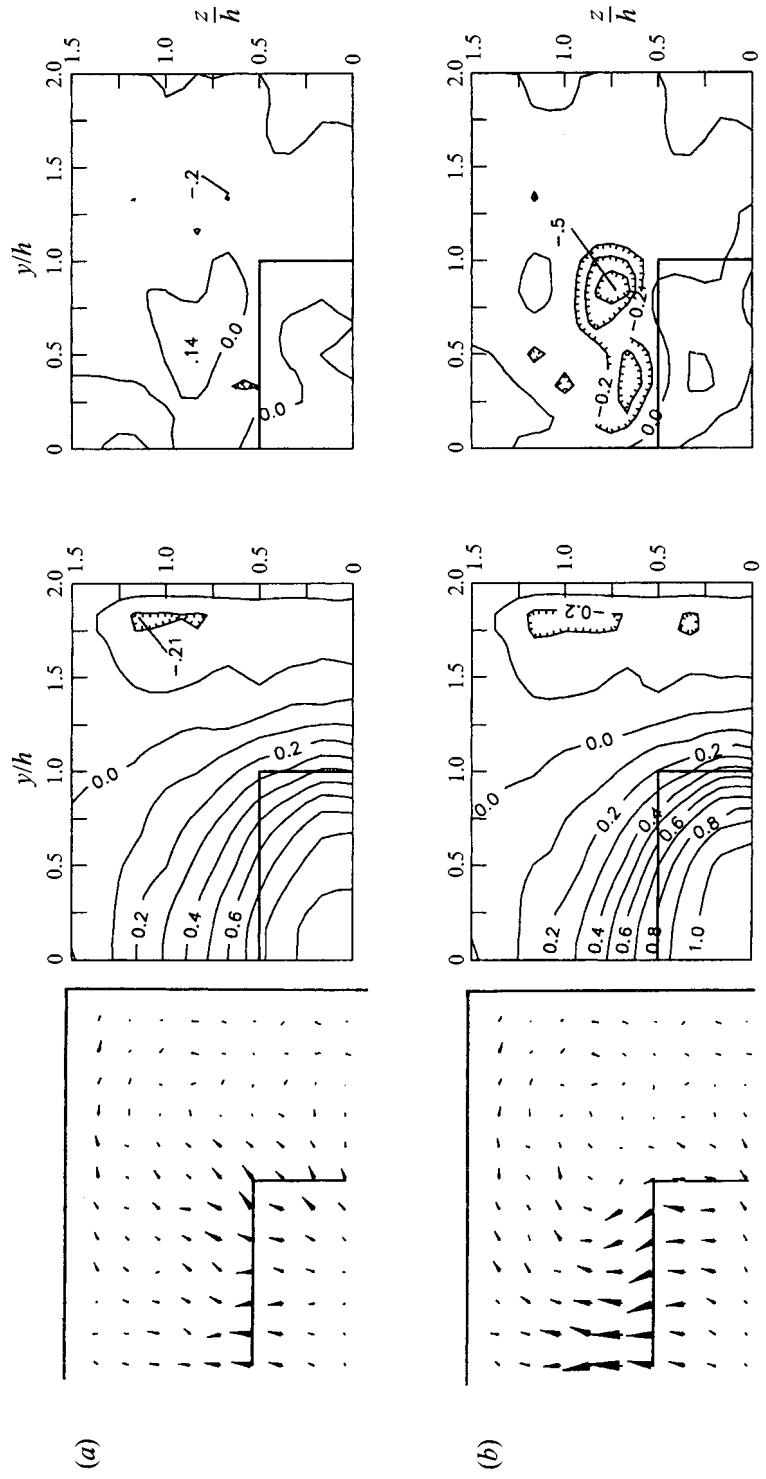
(a)
(b)
y/h
z/h
0
0.5
1.0
1.5
2.0
-.21
-.2
.14
0.0
-.5
-0.2
0.2
0.4
0.6
0.8
1.0

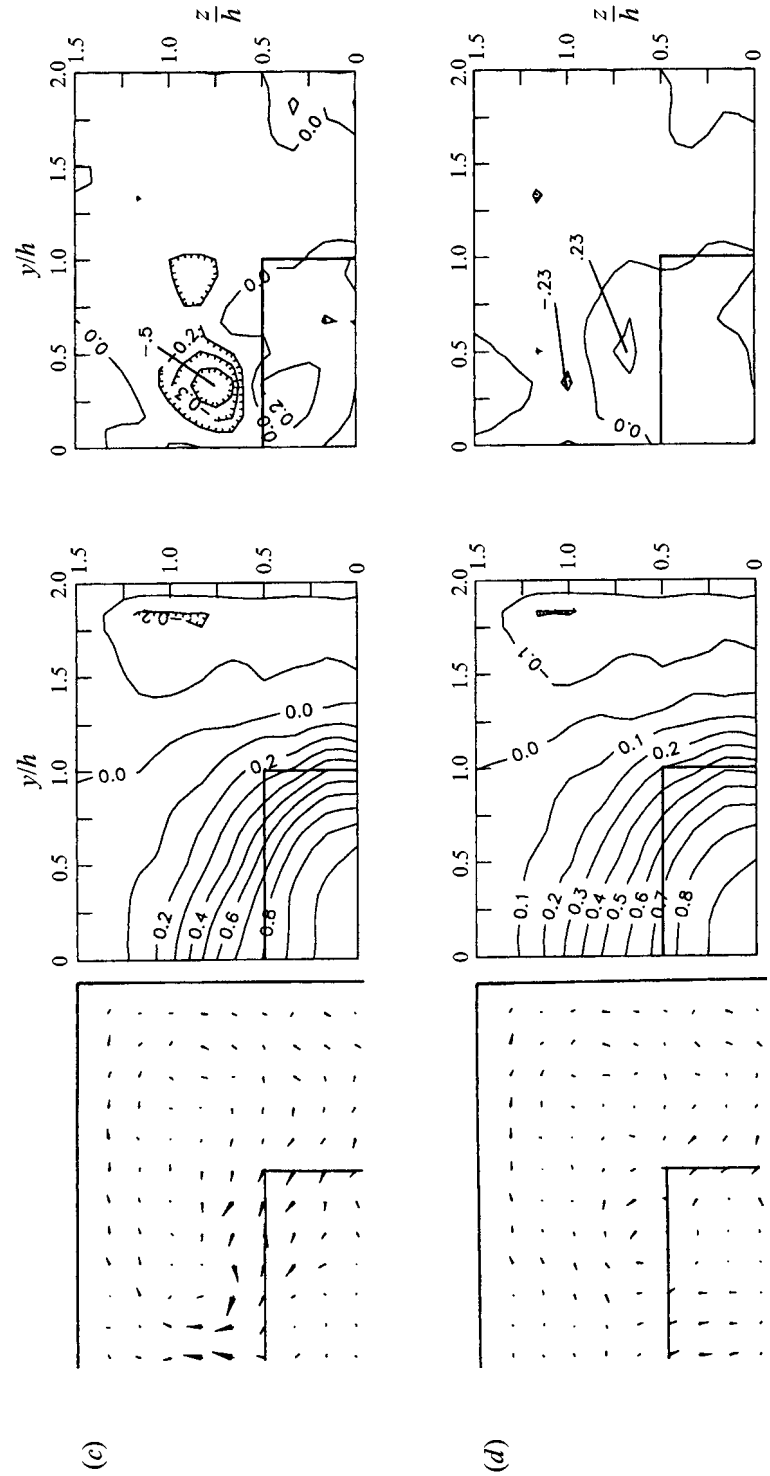

FIGURE 13. Velocity vectors V and W (left plots), contours of U/U_0 (middle plots) (contour interval = 0.1), and contours of $\omega_x h/U_0$ (right plots) (contour interval = 0.2), at $x/h = 3.0$: (*a*) 0°, (*b*) 90°, (*c*) 180°, (*d*) 270°.

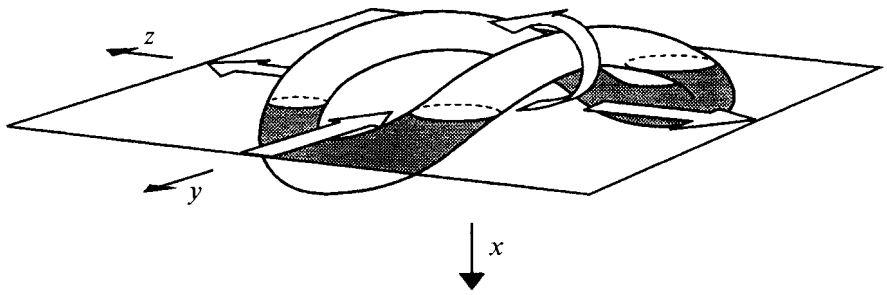

FIGURE 14. Vortex ring deformation at $x/h = 3$, between 90° and 180°.

and the vorticity contours. The core of the ring on the major axis passes through the plane at 90° through the forcing cycle, while the core on the minor axis passes through at 180°.

Figure 13 shows that at 0° there is outward flow on both the major and minor axes as the vortex ring approaches. There is little streamwise vorticity at this phase in the cycle. At 90°, the core of the ring is passing through the plane on the major axis, and the outward flow on the major axis has decreased accordingly. Outward flow on the minor axis, on the other hand, has increased, as is expected from the approach of the vortex core. In addition, significant negative streamwise vorticity is seen at $(y, z) = (-0.75, -0.75)$. This is consistent with a vortex ring deformation shown schematically in figure 14. At 180°, the back side of the vortex ring causes inward flow on the major axis. Passage of the core on the minor axis causes diminished outward flow there. The peak of the streamwise vorticity has moved close to the minor axis. At 270°, the flow on the minor axis is inward, due to the back side of the vortex. Little streamwise vorticity is found at this phase, indicating that any 'braid' type structures in the shear layer are not consistent enough in phase or position to be apparent.

As the next vortex ring approaches the lower measurement plane, a strong outward flow is seen, beginning again on the minor axis at 0°. This outward flow is then deflected by the walls into the outer corner, resulting in the low-level negative vorticity found throughout the recirculation zone.

The passage of the ring through the plane at $x/h = 3$ between 90° and 180° is consistent with the locations of the vortex cores in the symmetry planes, seen in figures 6 and 7. Given the convection velocity of the structures, the major axis region is leading by $0.5h$. This corresponds roughly to the deformation seen in the isolated ring in figure 3(*b*). However, the isolated ring achieves this shape within 1.5 step heights. At $x/h = 3$ the isolated ring has already undergone significant wall interaction and further deformation, while for the forced steady jet the ring is still $0.5h$ from the wall in the minor axis plane.

Not all of the transverse flows in the upper or lower measurement planes are associated with the passage of the vortex structure. Throughout the cycle there is consistent negative $-V$ flow parallel to the major axis in the upper plane (figure 12), particularly from $y/h = 0.5$ to 1.5, $z/h = 0.75$ to 1.5. This is associated with the secondary flow system. Near the step, fluid from the recirculation zone is convected into the region near the minor axis, where a portion is entrained into the vortex structure and the rest is turned into the positive flow seen behind the step on the minor axis plane. This flow is the source for the increased flow rate on the minor axis. This consistent negative-V flow also appears to be responsible for the consistent positive peak of ω_x found just outside the shear layer at $y/h = 0.7$, $z/h = 0.6$. In the lower plane (figure 13) there is consistent flow along the wall from the minor axis region into the

recirculation zone, as the rapidly spreading jet on the minor axis encounters the confining wall. There is also little transverse flow elsewhere in the recirculation zone, indicating that the 'sink' for both the fluctuating and time-averaged transverse flows must be in the streamwise direction. Thus the deformation of the vortex ring drives the time-averaged transverse flows both directly, through high entrainment near the step in the minor axis region, and indirectly, as the rapidly spreading jet displaces fluid into the recirculation zone, where it is returned to the region behind the step on the minor axis.

Rectangular channel flows are known to generate streamwise corner vortex pairs, and such vortices might have been generated in the rectangular inlet channel, upstream of the sudden expansion. However, none were observed in the transverse plane measurements just downstream of the expansion (figure 12). This result was not unexpected, since such corner vortices require long development distances, while in this configuration a length of only 4.5 step heights existed in the upstream channel between the upstream contraction and the expansion plane.

4. Concluding remarks

The time-averaged results (Hertzberg & Ho 1992) for this flow configuration showed how a small deviation from a two-dimensionally symmetric flow can completely change the global features. In this confined rectangular sudden expansion significant transverse velocities are found which have no parallel in axisymmetric or plane symmetric expansions. A phase-locked analysis has shown how the fluctuating components of these transverse flows can be directly related to the three-dimensional behaviour of vortex structures formed in the confined jet's shear layers. The dependence of the non-fluctuating transverse velocity components on the vortex structure deformation is less direct.

Closer examination of the vortex dynamics in the shear layers of a rectangular sudden expansion has revealed behaviour similar in some ways to that of an isolated vortex ring in this configuration. The vortex core in the major axis plane remains on a line with the step edge, while the vortex moves outward on the minor axis, although not as much as in the isolated ring case. Deformation of the vortex ring in the x-direction is also found in both the isolated ring and steady-state jet cases, with the isolated ring again showing the more dramatic behaviour. The deformation in both cases is consistent with the effects of self-induction. In addition, the deformation in the steady-state case is suggested as contributing to the development of streamwise vorticity in the shear layer, both directly and indirectly through entrainment effects which drive the secondary flow.

The unusual time-averaged secondary flow may thus be indirectly related to the vortex structure dynamics. As in elliptic free jets, the confined rectangular jet spreads more rapidly on the minor axis. This is likely due to the self-induced vortex structure deformation, as documented in the vortex trajectory data. In this confined case, the spreading will displace fluid from the minor axis region into the recirculation zone on the major axis. Behind the step, this recirculated fluid is returned to the minor axis region, where a portion is entrained into the jet, and the rest is deflected into streamwise flow by the confining walls.

Additional experiments are underway to examine the effects of premixed combustion on the three-dimensional flow field of this configuration.

This work was supported by a University Research Initiative contract from the

Office of Naval Research, and a Research Initiation Grant from the National Science Foundation.

REFERENCES

ADAMS, E. W., JOHNSTON, J. P. & EATON, J. K. 1984 Experiments on the structure of turbulent reattaching flow. Thermosciences Division, Department of Mechanical Engineering, Stanford University, MD-43.

BHATTACHARJEE, S., SCHEELKE, B. & TROUTT, T. R. 1986 Modification of vortex interactions in a reattaching separated flow. *AIAA J.* **24**, 623–629.

CHERDRON, W., DURST, F. & WHITELAW, J. H. 1978 Asymmetric flows and instabilities in symmetric ducts with sudden expansions. *J. Fluid Mech.* **84**, 13–31.

CRIGHTON, D. G. 1973 Instability of an elliptic jet. *J. Fluid Mech.* **59**, 665–672.

DURST, F., MELLING, A. & WHITELAW, J. H. 1981 *Principles and Practice of Laser-Doppler Anemometry*, 2nd edn, pp. 271–273. Academic.

EATON, J. K. & JOHNSTON, J. P. 1981 A review of research on subsonic turbulent flow reattachment. *AIAA J.* **19**, 1093–1100.

FOSS, J. F. & JONES, J. B. 1968 Secondary flow effects in a bounded rectangular jet. *Trans. ASME* D: *J. Basic Engng* June, 241–248.

GRINSTEIN. F. F. & KAILASANATH, K. 1993 Dynamics of spatially developing reactive square jets. *Ninth Symp. on Turbulent Shear Flows, Kyoto, Japan, August 16–18, Paper* 25–4.

GUTMARK, E. & HO, C. M. 1986 Visualization of a forced elliptic jet. *AIAA J.* **24**, 684–685.

HERTZBERG, J. R. & HO, C. M. 1992 Time-averaged three-dimensional flow in a rectangular sudden expansion. *AIAA J.* **30**, 2420 (and errata **30**, 2803).

HILEY, P. E., WALLACE, H. W. & BOOZ, D. E. 1976 Nonaxisymmetric nozzles installed in advanced fighter aircraft. *J. Aircraft* **13**, 1000–1006.

HO, C. M. & GUTMARK, E. 1987 Vortex induction and mass entrainment in a small-aspect-ratio elliptic jet. *J. Fluid Mech.* **179**, 383–405.

HO, C. M. & HUANG, L. S. 1982 Subharmonics and vortex merging in mixing layers. *J. Fluid Mech.* **119**, 443–473.

HO, C. M. & HUERRE, P. 1984 Perturbed free shear layers. *Ann. Rev. Fluid Mech.* **16**, 365–424.

HO, C. M. & NOSSEIR, N. S. 1981 Dynamics of an impinging jet. Part 1. The feedback mechanism. *J. Fluid Mech.* **105**, 119–142.

HOLDEMAN, J. D. & FOSS, J. F. 1975 The initiation, development and decay of the secondary flow in a bounded jet. *Trans. ASME* I: *J. Fluids Engng* **97**, 342–352.

HOYT, J. W. & TAYLOR, J. J. 1978 Elliptical water jets. *AIAA J.* **16**, 85–87.

HSIA, Y., KROTHAPALLI, A., BAGANOFF, D. & KARAMCHETI, K. 1983 Effects of mach number on the development of a subsonic rectangular jet. *AIAA J.* **21**, 176–177.

HUSAIN, H. S. & HUSSAIN, F. 1991 Elliptic jets. Part 2. Dynamics of coherent structures: pairing. *J. Fluid Mech.* **233**, 439–482.

HUSSAIN, F. & HUSAIN, H. S. 1989 Elliptic jets. Part 1. Characteristics of unexcited and excited jets. *J. Fluid Mech.* **208**, 257–320.

KAMBE, T. & TAKAO, T. 1971 Motion of distorted vortex rings. *J. Phys. Soc. Japan* **31**, 591–599.

KROTHAPALLI, A. 1985 Discrete tones generated by an impinging underexpanded rectangular jet. *AIAA J.* **23**, 1910–1915.

KROTHAPALLI, A., BAGANOFF, D. & KARAMCHETI, K. 1990 Development and structure of a rectangular jet in a multiple jet configuration. *AIAA J.* **18**, 945–950.

KROTHAPALLI, A., BAGANOFF, D. & KARAMCHETI, K. 1981 On the mixing of a rectangular jet. *J. Fluid Mech.* **107**, 201–220.

MORRISON, G. L., TATTERSON, G. B. & LONG, M. W. 1988 Three-dimensional laser velocimeter investigation of turbulent, incompressible flow in an axisymmetric sudden expansion. *J. Propulsion* **4**, 533–540.

NAKAO, S. 1986 Turbulent flow in square ducts after an expansion. *AIAA J.* **24**, 979–982.

POLLARD, A. & SCHWAB, R. R. 1988 The near-field behavior of rectangular free jets: An

experimental and numerical study. In *Experimental Heat Transfer, Fluid Mechanics and Thermodynamics* (ed R. K. Shah, E. N. Ganić & K. T. Yang) Elsevier.

QUINN, W. R. 1992 Streamwise evolution of a square jet cross-section. *AIAA J.* **30**, 2852–2857.

RAYLEIGH, LORD 1879 On the capillary phenomena of jets. *Proc. R. Soc. Lond.* **29**, 71–91.

ROOS, F. W. & KEGELMAN, J. T. 1986 Control of coherent structures in reattaching laminar and turbulent shear layers. *AIAA J.* **24**, 1956–1963.

SCHADOW, K. C. & GUTMARK, E. 1992 Combustion instability related to vortex shedding in dump combustors and their passive control. *Prog. Energy Combust. Sci.* **18**, 117–132.

SHIMUZU, A., ISHII, H. & WADA, T. 1986 A numerical analysis of vortex growth in a bounded rectangular jet. *Computers Fluids* **14**, 327–359.

SFEIR, A. A. 1976 The velocity and temperature fields of rectangular jets. *Intl J. Heat Transfer* **19**, 1289–1297.

SFEIR, A. A. 1979 Investigation of three-dimensional Turbulent rectangular jets. *AIAA J.* **17**, 1055–1060.

SFORZA, P. M. & STASI, W. 1979 Heated three-dimensional turbulent jets. *Trans. ASME* C: *J. Heat Transfer* **101**, 353–358.

SFORZA, P. M., STEIGER, M. H. & TRENTACOSTE, N. 1966 Studies on three-dimensional viscous jets. *AIAA J.* **4**, 800–806.

STEVENSON, W. H., THOMPSON, H. D. & CRAIG, R. R. 1984 Laser velocimeter measurements in highly turbulent recirculating flows. *Trans. ASME* D: *J. Fluids Engng* **106**, 173–180.

STEVENSON, W. H., THOMPSON, H. D. & ROESLER, T. C. 1986 Direct measurement of laser velocimeter bias errors in a turbulent flow. *AIAA J.* **20**, 1720–1723.

TROUTT, T. R., SCHEELKE, B. & NORMAN, T. R. 1984 Organized structures in a reattaching separated flow field. *J. Fluid Mech.* **143**, 413–427.

TSUCHIYA, Y., HORIKOSHI, C. & SATO, T. 1986 On the spread of rectangular jets. *Exp. Fluids* **4**, 197–204.

VIETS, H. 1972 The three-dimensional laminar elliptical laminar jet in a coflowing stream. *NTIS ARL* 72-0052.

VIETS, H. 1976 Approximate analysis of a laminar elliptic jet. *AIAA J.* **14**, 129–130.

WU, C.-K., CHEN, L.-F., LI, J., WANG, H.-Y., WEI, J.-B., ZHAN, H.-Q. & ZHU, F.-Y. 1988 The use of nonsymmetrical jets for the stabilization of low grade coal flames. *Twenty Second Symposium (Intl) on Combustion*, pp. 193–199. The Combustion Institute.